AIMS Materials Science, 13(1): 1–29.
DOI: 10.3934/matersci.2026001
Received: 01 September 2025
Revised: 18 November 2025
Accepted: 05 December 2025
Published: 23 December 2025

https://www.aimspress.com/journal/Materials

Research article

Effect of the sea breeze on the durability of pumice-based supersulfated pastes under accelerated conditions

Kenson Noel[1,2], David Reyes-Gonzalez[1,*], Rodrigo Vivar-Ocampo[3], Pablo J. Lopez-Gonzalez[1] and Gustavo Martinez Castellanos[1]

[1] Postgraduate Studies and Research Department, TecNM, Misantla Campus, Veracruz, Mexico
[2] Postgraduate Studies and Research Department, TecNM, Teziutlan Campus, Puebla, Mexico
[3] Renewable Energy Department, Autonomous University of Baja California, Mexico

* **Correspondence:** Email: dreyesg@itsm.edu.mx.

Abstract: In this study, we investigated the mechanical performance and durability of supersulfated pastes (SSP) formulated with locally sourced pumice (PM) activated by a two-stage NaOH process, proposed as a low-carbon alternative to Portland cement (PC) for protective coatings in marine environments. The novelty of this work lies in the development of a supersulfated paste for coating that uses local pumice activated with NaOH as the main cementitious material, reaching PC substitutions up to 50%. Seven formulations were prepared, including a PC control, with varying proportions of PM, PC, hemihydrate, and $Ca(OH)_2$, cured for 28, 56, and 90 days, and subsequently exposed to an accelerated regimen of marine aerosols. Compressive strength, carbonation depth, chloride penetration, and moisture absorption were quantified as key indicators of durability. According to the results, SSP consistently outperformed PC control in all four durability parameters. Statistical analysis confirmed significant improvements in carbonation resistance, chloride resistance, and moisture absorption from 56 days after curing. Overall, SSP containing 30% PC, and 70% supersulfated components (SC), as well as those with 40% PC and 60% SC, demonstrated superior strength and durability compared to the control sample. In addition, the properties of the supersulfated pastes improved markedly after 56 days, cementing their potential as durable coating materials for coastal environments.

Keywords: accelerated breeze; durability; compressive strength; supersulfated pastes; absorption

1. Introduction

Concrete is the most widely used building material in infrastructure worldwide, mostly due to the adhesiveness and versatility provided by Portland cement [1]. However, this material is susceptible to structural failures caused by external stresses and chemical attacks, especially in aggressive environments such as maritime, which requires constant maintenance interventions to preserve its functionality and durability [2]. Among the strategies to protect concrete from these challenges, epoxy coatings, waterproofing, resins, corrosion inhibitors and the use of sulfate-resistant cements stand out [3]. In the state of Veracruz, Mexico, homes experience accelerated deterioration due to the constant action of the sea breeze, which directly affects the concrete that protects the reinforcing steel in the structural elements. Once the concrete cracks or crumbles, moisture and salt agents corrode the embedded steel, causing widespread damage. The degradation process begins in early stages: In less than 10 months after construction, problems such as carbonation of the concrete, detachment of the coating, oxidation of the steel, and loss of section in the rods due to corrosion are evident. To mitigate these damages, the conventional methods most used in the area include the application of Portland cement mortars or pastes or coatings with paints and epoxy resins. These interventions must be carried out, on average, twice a year, which implies a significant expenditure on maintenance for the inhabitants of the region.

To significantly enhance the durability of conventional cement-based materials, such as mortars and concretes, exposed to severe environments like marine zones, research over the past two decades has increasingly focused on the use of pozzolanic materials as sustainable alternatives for the partial replacement of Portland cement [4–6]. In addition to reducing the environmental footprint of cement, which accounts for more than 7% of global CO_2 emissions and approximately 3% of worldwide energy consumption [7], industrial (granulated slag, fly ash, silica fume) and natural pozzolans (pumice, zeolite, metakaolin, natural pozzolana, perlite) have demonstrated the ability to improve chemical resistance and long-term durability in cementitious matrices [8,9]. Researchers further confirm the high pozzolanic reactivity of natural materials, such as perlite and natural pozzolana, as well as their capacity to control alkali-silica reaction [10,11] and promote self-healing in mixtures with high substitution levels [12]. Among the most extensively investigated alternative binders are supersulfated cements (SSC), known for their high resistance to sulfate and chloride attack [13,14], prolonged durability in marine environments through alkalinity regulation [15], and effective mitigation of alkali-silica reaction [11]. Their sustainability arises from the fact that they do not require high-temperature calcination and can act as chemical barriers against chloride ions and CO_2, extending the service life of structures in aggressive environments [16]. Research on sulfate-resistant materials also includes other alternative binders. Studies on calcium sulfoaluminate (CSA) cements have shown that polymer-modified formulations [17,18] enhance microstructural density and resistance to aggressive ions. Likewise, alkali-activated materials (geopolymers) show high sulfate resistance due to their stable aluminosilicate matrix [19]. These advances converge on the need to optimize microstructure to create effective protective barriers, a principle applied in the present study through the design of pumice-based supersulfated matrices for marine environments.

However, the production of conventional SSC depends heavily on the availability of granulated blast furnace slag, which restricts their application in regions where this industrial by-product is scarce or economically inaccessible. This limitation has driven the development of natural-pozzolan-based SSC, including pumice-derived systems, which have shown promising performance in novel supersulfated

formulations [20]. In Si-A-rich systems such as pumice-based binders, the synergistic formation of nanostructured ettringite and C-A-S-H gels has been shown to reduce permeability and significantly improve durability in supersulfated matrices [14,21]. The performance of SSC is governed largely by the formation and long-term stability of ettringite, which is controlled by the chemical balance of the matrix [22]. While higher Al_2O_3 contents promote the formation of acicular ettringite (1–5 μm), systems with high SiO_2/Al_2O_3 ratios (>3), typical of siliceous natural pozzolans, favor nanostructured ettringite (20–50 nm) encapsulated within C-A-S-H gels, reducing pore connectivity and enhancing durability. In addition, parameters such as the Al_2O_3/SO_3 ratio (>1.5) are critical to prevent ettringite conversion to monosulfate and maintain volumetric stability [23].

Despite these advances, a critical gap remains: the mechanisms governing how alkaline activation of a natural pozzolan with the specific chemistry of pumice regulates initial dissolution, early hydration product formation, and the long-term stability of ettringite under accelerated marine exposure cycles have not been fully elucidated.

In this context, we introduce a novel approach through the development of a supersulfated coating paste formulated with locally sourced pumice, activated with NaOH, and optimized for the coastal conditions of Veracruz. The mixtures incorporated varying proportions of activated pumicite, reaching up to 50 wt% in some formulations, and were combined with a controlled two-stage alkaline activation procedure and an accelerated marine aerosol exposure protocol. This methodology aims to provide a more effective and sustainable barrier against chloride ingress and carbonation [24], overcoming the durability limitations of Portland cement in this environment.

The selection of pumice was based not only on its local availability which reduces transportation-related carbon emissions, but also on its chemical composition (Table 1). Its high amorphous SiO_2 content (72.8%) and Al_2O_3 content (11.8%) identify it as a rhyolitic pozzolan with a SiO_2/Al_2O_3 ratio of approximately 6.2, an optimal condition for promoting the simultaneous formation of C-S-H and C-A-S-H gels in sulfated media, contributing to a dense and durable microstructure according to [14,25]. Regarding activation, sodium hydroxide (NaOH) was selected due to its proven effectiveness in dissolving the aluminosilicate glass phases of pumice, releasing reactive species such as $[SiO(OH)_3^-]$ and $[Al(OH)_4^-]$ required for polycondensation and subsequent ettringite formation in the presence of calcium sulfate [26,27].

2. Materials and methods

2.1. Materials

In this work, the following materials were used in different proportions for supersulfated pastes: pumice (PM), Portland cement (PC), hemihydrate ($CaSO_4 \cdot ½H_2O$), and calcium hydroxide ($Ca(OH)_2$).

2.1.1. PM characterization

The pumice used in this study was obtained from volcanic deposits in Perote, Veracruz (19º35'18"N, 97º13'31"W). The material was first characterized by X-ray diffraction (XRD, Bruker, D2 Phaser Diffractometer) using a Cu-Kα radiation source in a range of 7° to 100° 2θ with a step size of 0.018° 2θ and a wavelength of 1.5406 Å, to identify its mineralogical phases. The resulting diffractogram, presented in Figure 1, shows a characteristic amorphous halo typical of volcanic glass,

consistent with the amorphous structure of pumice reported in the literature for similar materials [28]. This confirms the predominantly vitreous and reactive nature of the pumice used.

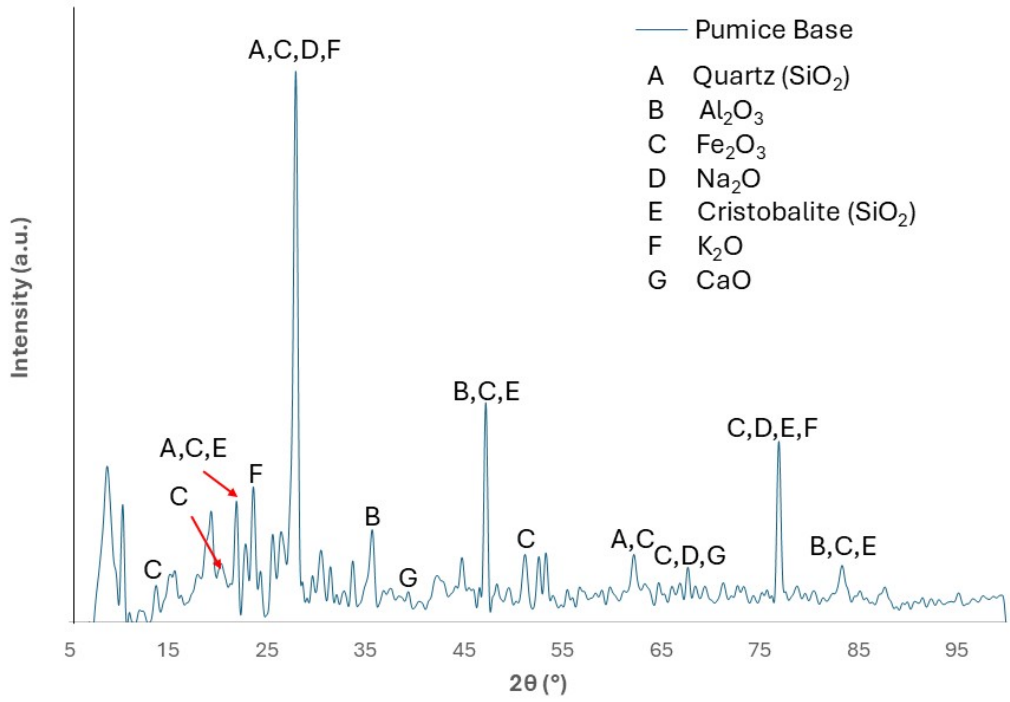

Figure 1. XRD pattern and mineral phases present in PM.

Regarding the chemical composition, since the pumice under study originates from the same deposit and batch as the material fully characterized by [29], we directly adopted the oxide composition obtained by X-ray Fluorescence (XRF) from that previous study. This approach avoids redundant analysis and ensures consistency with data for the same material. The chemical composition of the PM and PC is summarized in Table 1.

Table 1. Chemical composition of major oxides (wt%) of raw materials by XRF [29].

Material	SiO_2	Al_2O_3	Fe_2O_3	CaO	K_2O	Na_2O	SO_3	MgO	Others
Portland cement	18.47	4.13	3.80	65.31	1.13	0.46	4.64	1.42	0.64
Pumice	72.8	11.8	7.2	0.7	1.0	4.2	---	---	---

The chemical composition of the PM used in this study, shown in Table 1, contains the same major oxide components as Portland cement, although in different proportions. This compositional similarity suggests that pumice may demonstrate cementitious behavior comparable to PC. Additionally, the researchers in [14] reported that the PM employed here has a surface area of 500 m^2/kg and an average particle size of 12 μm, which are characteristic of rhyolitic pozzolanic materials. The material was subjected to sequential crushing until a powder with 100% passing through the No. 200 sieve (75 μm) was obtained, following the sieving requirements of ASTM C136/C136M-19.

2.1.2. Characterization of the other components

Sodium hydroxide (NaOH, 97% purity, WÖHLER) was used as the alkaline activator for the pumice due to its high efficiency in dissolving silica and alumina and promoting the formation of cementitious phases. Compared with other alkaline activators, Na^+ cations have a smaller ionic radius and therefore exhibit higher mobility within the matrix, which enhances overall reactivity [30]. According to [31], NaOH rapidly increases the system's pH, enabling the dissolution of the vitreous structure of pumice and the release of silicate and aluminate ions, which are essential precursors for the formation of C-A-S-H gels and ettringite in supersulfated environments. It also regulates pore solution alkalinity and influences the stability of hydrated phases. A 0.5 N concentration of NaOH was selected, as this level represents an optimal balance [31]: it is sufficiently strong to promote effective pumice reactivity while avoiding excessive alkalinity, efflorescence, or instability of the resulting hydration products, consistent with researchers using similar aluminosilicate precursors.

The PC used in this work, whose chemical characterization is presented in Table 1, is a Portland Composite Cement CPC 30 R (CEMEX, Mexico). This cement complies with the specifications of the Mexican Standard NMX-C-414-ONNCCE-2014 and is classified as a rapid-strength cement, achieving compressive strengths ≥30 MPa at 28 days. Its chemical composition, reported in [29], is consistent with the manufacturer's technical data, confirming the reliability of the material used. As shown in Table 1, the cement shows a high calcium oxide content (CaO = 65.31% by mass), which is typical of Portland clinker phases and is primarily responsible for the hydration reactions that generate C-S-H gel and portlandite, the phases governing the mechanical performance and early-age strength development of PC-based matrices [32]. Additionally, the presence of SiO_2, Al_2O_3 and Fe_2O_3 within the characteristic ranges further confirms the material's conformity with standard Portland formulations.

The hemihydrate ($CaSO_4 \cdot ½H_2O$) used in this study was a commercial product (Yeso Construcción HIDALGO, Mexico). Because the manufacturer does not report chemical purity, key physical properties were experimentally characterized following standardized procedures. Bulk density was measured according to ASTM C188, yielding 854.61 kg/m^3. Moisture absorption was determined by exposing an oven-dried sample to 75% relative humidity at 23 °C for 24 h, following the principles of ASTM C1498, resulting in an absorption of 0.054% by weight. Water absorption was quantified by immersing a pre-dried sample in distilled water for 24 h, following the general methodology of ASTM C642, obtaining a value of 48.62% by weight. Although chemical purity was not directly measured, these physical properties fall within the typical ranges reported for construction-grade hemihydrates [14,33], supporting the suitability of this material for the supersulfated paste formulations investigated in this study.

Finally, calcium hydroxide from the commercial brand CALIDRA was used. The bulk density of the material, experimentally determined in our laboratory according to the principles of ASTM C188, was 2240 kg/m^3, a value that coincides with the manufacturer's specifications. For other critical parameters that directly influence its function as an alkaline activator, such as the specific surface area (15–20 m^2/g) and the pH in suspension (12.4–12.6 at 20 °C), the technical specifications of the supplier were used, since it is a recognized manufacturer that guarantees the consistency of the product for industrial applications and because these parameters correspond to intrinsic properties controlled during its manufacture. The methodological approach focused on the fundamental physicochemical properties (density, surface area, and alkalinity), which govern the macroscopic behavior of the material in the paste. The chemical composition reported by the manufacturer (≥95% $Ca(OH)_2$, ≤3%

$CaCO_3$, ≤2% other oxides) was therefore considered adequate and consistent with our main objective of this work: to evaluate the overall performance of supersulfated pastes. Detailed mineralogical characterization and reactivity studies have been identified as key targets for future research. In this context, calcium hydroxide was used as an alkaline activator, favoring the dissolution of pozzolanic components and the formation of cementitious phases according to [34].

2.2. Design of mixtures and preparation of pastes

Table 2 shows the design of seven types of pastes: six supersulfated and one reference (control) paste, with their respective percentages in total mass; NaOH is used to activate pumice in supersulfated cement. Bulk densities of the sample components are detailed in Table 3.

Except for the control paste, made only with water and Portland cement, the supersulfated pastes followed a process that began with the activation of pumice with sodium hydroxide at a concentration of 0.5 N, functioning as a cementing agent in partial replacement of Portland cement. This was mixed with a variable proportion PC or $Ca(OH)_2$ being alkaline activators, and then $CaSO_4 \cdot ½H_2O$ was added, being the supersulfatic agent. Finally, water was added in the necessary quantities according to the specific water-cement ratio.

Table 2. Design of supersulfated and control mixtures (unit in percentage).

Pastes codes	PC	Pumice	NaOH	$CaSO_4 \cdot ½H_2O$	$Ca(OH)_2$
A-1	25	30	0.28	20	25
B-1	15	50	0.56	20	15
C-1	100	0	0	0	0
D-1	50	30	0.23	20	0
E-1	30	50	0.48	20	0
F-1	20	40	0.4	20	20
G-1	40	40	0.34	20	0

Table 3. Bulk densities of the sample components.

Bulk density (kg/m^3)	
NaOH	2130
$Ca(OH)_2$	2240
PC	3150
Pumice	980
$CaSO_4 \cdot ½H_2O$	854.61
Water	1000

Notably, each paste design required a specific water/cementitious (w/c) ratio, experimentally determined through successive adjustments to ensure optimal workability. Water content was incrementally added until simultaneously achieving three predefined criteria: (a) cohesion without exudation, (b) self-leveling time ≤35 s measured via mini-slump flow test, and (c) reproducibility with variation <5% in self-leveling time between replicate mixes. Among these, the self-leveling time

served as the dominant quantitative criterion for final selection, while cohesion provided essential qualitative verification. This adjustment technique followed methodologies validated for high-sulfate content pastes [34].

The w/c ratio was calculated considering the total mass of cementitious materials, including Portland cement and activated pumice, with the latter classified as a supplementary cementitious material due to its pozzolanic reactivity in the alkaline system. The variability in w/c ratios across paste designs primarily stems from the differential water demand of constituents, particularly the highly porous pumice powder (<75 μm), which exhibits greater water affinity to achieve adequate workability [35]. The exact proportions used in this study are detailed in Table 4.

Table 4. Water/cement ratio of the different designs of paste mixtures.

Pastes codes	Water/cement ratio
A-1	0.45
B-1	0.46
C	0.43
D-1	0.45
E-1	0.46
F-1	0.46
G-1	0.46

2.3. Mixing process

Once the w/c values were determined, the mixtures were prepared following the two-stage method proposed in [36]. Figure 2 shows the major components in the two-step process of supersulfated pulp production. The mixing process used in this work was carried out manually, applying the homogenization principles established in the ASTM C305-20 standard. Although this standard describes a protocol for mechanical mixing, its logical sequence and homogenization criteria were implemented in a controlled manner using a steel spatula and a metal tray. In the first stage, the pumice was impregnated with a solution of 0.5 N NaOH in a solid/liquid ratio of 0.6, activated in a thermostatic bath at 45 ± 2 °C for 30 min, with manual agitation every 10 min to promote the dissolution of silica and alumina, essential for the formation of cementitious phases in supersulfated systems [37]. In the second stage, the activated suspension was transferred to the tray, first incorporating the hemihydrate ($CaSO_4 \cdot ½H_2O$) by two minutes of vigorous mixing until a uniform dry mixture was obtained; subsequently, Portland cement and, where appropriate, $Ca(OH)_2$ were added, in accordance with the dosage established in the design of supersulfated and control mixtures presented in Table 2, mixing for an additional three minutes. The dry mixture was arranged in the shape of a volcano, the dosing water was gradually added, and an intensive five-minute kneading was carried out by folding, compression, and cutting to ensure complete homogenization. Workability was immediately verified by means of the mini-cone, meeting the self-leveling criterion ≤35 s. Finally, the pastes were placed in 50 mm cubic molds and compacted into two layers following the NMX-C-161-ONNCCE-2020 standard; they were then covered to prevent moisture loss and cured at 35 ± 2 °C for 24 h before demolding. The next day, the samples were carefully demolded and moved to their corresponding curing solutions.

The samples were subjected to two differentiated curing regimes designed to promote the optimal development of their cementitious properties. The reference (C-1) pastes, made from 100% Portland cement, were cured in a solution of water with 5% lime by mass, following the criteria established in standards for preserving alkalinity in cementitious matrices, such as the principles of ASTM C192/C192M-19. In contrast, the supersulfated pastes were cured in a 5% calcium sulfate ($CaSO_4 \cdot 2H_2O$) solution by mass. This regime, according to [14], is essential in supersulfated cements because it guarantees a continuous availability of sulfate ions (SO_4^{2-}), essential for the formation and stability of etringite, a key phase for the strength and durability of these systems. In this study, the successful use of a 5% $CaSO_4$ solution ensured sustained etringite formation in pumice-based supersulfated cements. In a complementary manner, [38] demonstrated that the availability of sulfate in the curing medium is a critical factor for the development of a dense and resistant microstructure in these materials. All curing solutions were renewed every 7 days to maintain a constant ionic concentration and ensure stable and reproducible curing conditions during the established periods of 28, 56 and 90 days. The mixing and curing process was carried out in the laboratory at an average ambient temperature of 35 ± 2 °C.

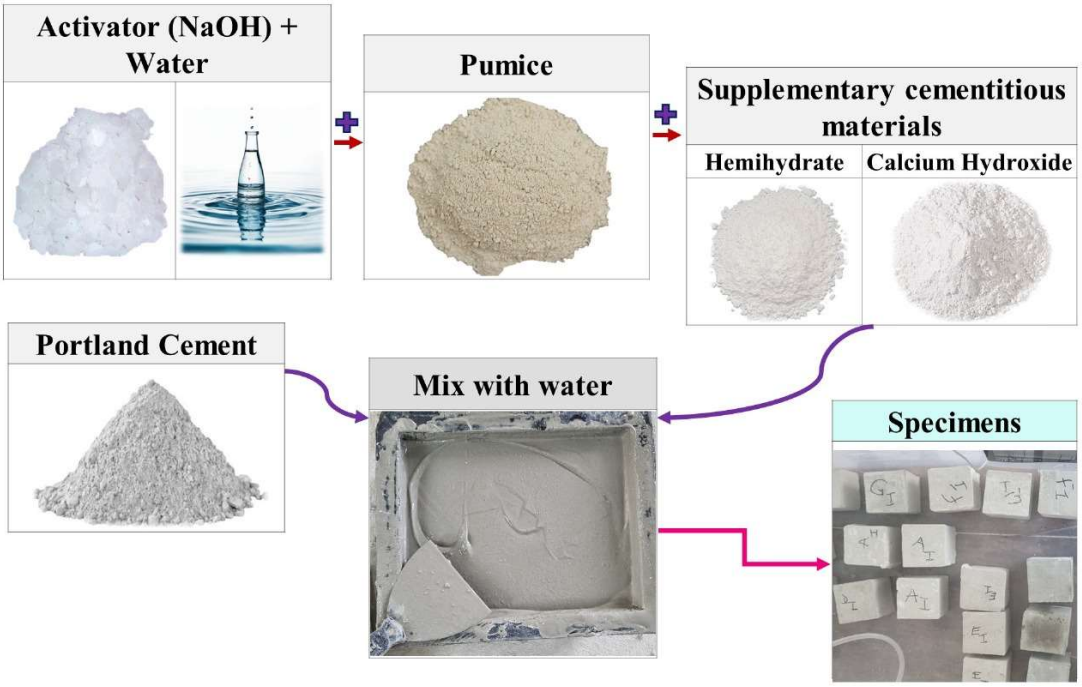

Figure 2. Mixing procedure for the main components of the supersulfated mixture.

According to [36], two-stage activation enhances the formation of cementitious phases compared to direct activation, as these gels can significantly improve durability by reducing permeability and increasing chemical resistance to aggressive agents such as sulfates and chlorides. The researchers in [39] showed that the two-part method can offer better mechanical properties, reaching compressive strengths above 60 MPa, good flexural and tensile strength, as well as outstanding durability against chemical attacks (acids, chlorides, and sulfates), high thermal resistance and low permeability, making it ideal for demanding conditions such as maritime infrastructures or aggressive environments. In contrast, based on [40], the one-part method, which uses solid activators and requires only adding

water on site, is more economical and environmentally friendly, although traditionally it had lower mechanical strengths, which have improved significantly in recent years thanks to advanced formulations.

2.4. Environmental and seawater characterization of the study region

A basic characterization of seawater was carried out in the central-coastal region of the state of Veracruz, Mexico. To do this, a portable multifunctional meter (model PH-786, type 6 in 1) was used, designed to record physicochemical parameters in real time, including pH, electrical conductivity (EC), total dissolved solids (TDS), salt content (SAL), specific gravity (S.G.), and temperature. Figure 3 shows the apparatus taking readings in the seawater of the study site.

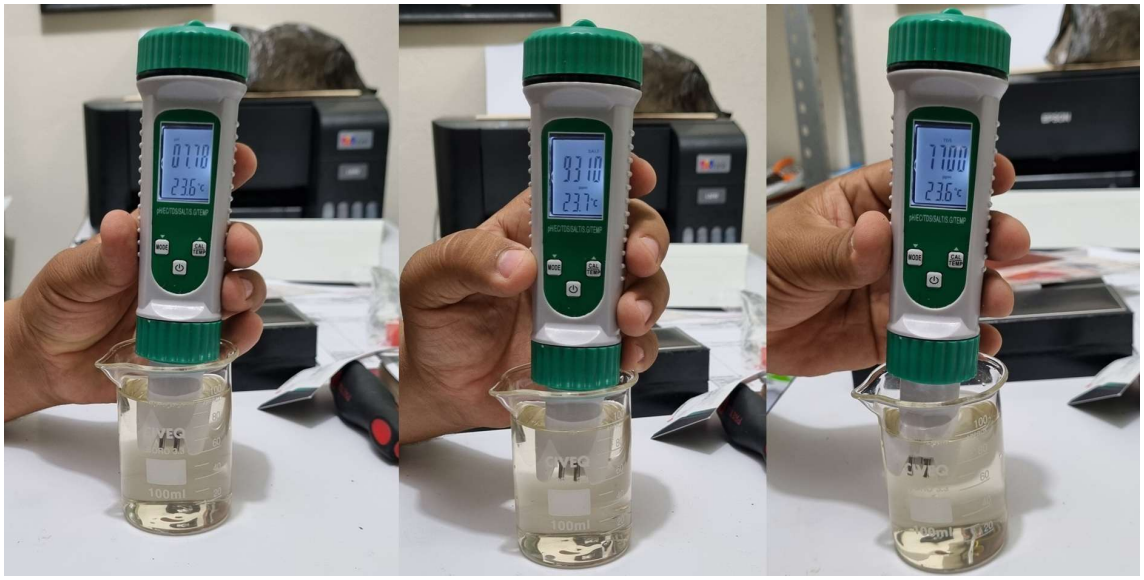

Figure 3. Obtaining the pH level, SAL, and TDS of seawater.

The measurements obtained in the laboratory for the seawater of the study area were: pH = 7.78, TDS = 7700 ppm, and total salt content = 9310 ppm (equivalent to 0.931 %) (Figure 3). From these data and following standard seawater composition criteria, the chloride ion content was estimated. Scientific sources agree that sodium (Na^+) and chloride (Cl^-) ions represent approximately 91% of TDS in seawater, with chloride being the predominant ion, constituting about 55% by mass of total salinity [41,42]. Applying this criterion, the approximate chloride content was estimated using the expression: Cl^- (mg/L) ≈ 0.55 × 9310 mg/L ≈ 5120.5 mg/L. This is equivalent to 5120.5 ppm Cl^-, assuming a 1:1 ratio between mg/L and ppm in aqueous solutions. This estimate is suitable for exploratory water quality studies, especially in coastal areas influenced by marine and fluvial waters. It should be added that a concentration of 5120.5 ppm of chloride ions represents a significant risk to the durability of reinforced concrete, since studies establish that corrosion of reinforcing steel can be initiated when the concentration of soluble chlorides exceeds 500 to 1000 ppm, equivalent to 0.05%–0.1% by mass with respect to the cement content in the mixture [43–45].

The main function of the supersulfated pastes of this work is to act as coatings for reinforced concrete elements in maritime environments, reducing their deterioration by salts and the atmospheric conditions of these areas. Figure 4 illustrates the superposition of this coating on the structural elements.

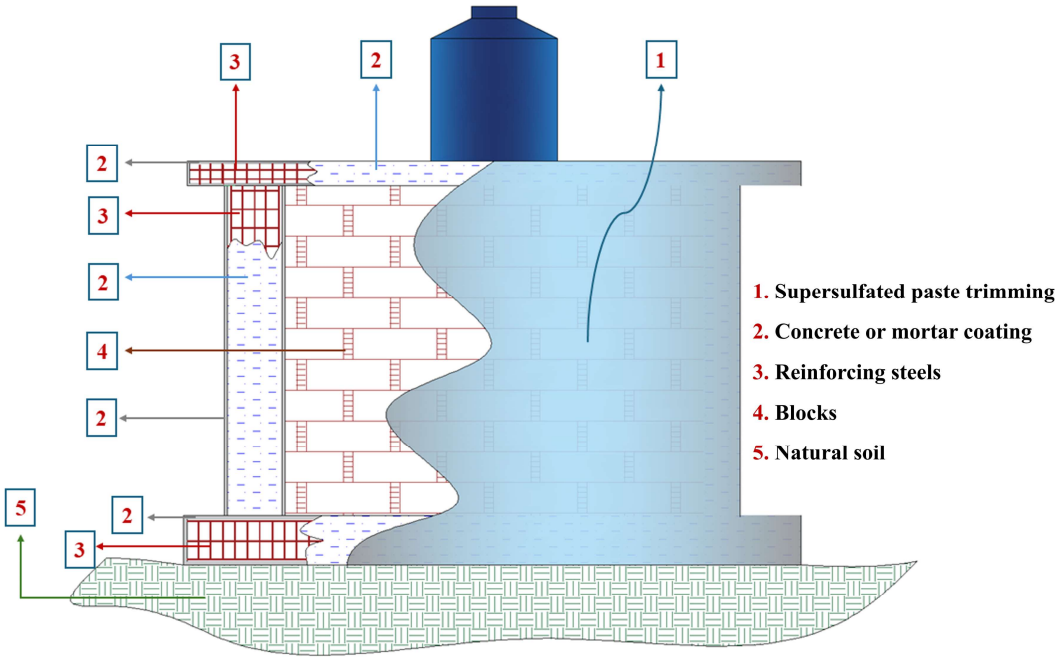

Figure 4. Structural system overview and proposed coating made with supersulfated pastes.

Figure 4 highlights the design of a typical structural system of the houses under study, which are exposed to deterioration processes induced by the action of the sea breeze. The illustration emphasizes, in bluish-gray color, the proposed supersulfated paste coating, which will be applied integrally to all structural elements. This coating functions as an additional physical and chemical barrier aimed at reducing the rate of penetration of aggressive agents present in the marine atmosphere, mostly chloride and sulfate ions. The intention was to mitigate this deterioration to prevent early corrosion of the embedded steel, thus contributing to the extension of the service life of the structural system [46].

2.5. Exposure of samples to simulated sea breezes

The procedure was designed following criteria used in accelerated durability studies in maritime environments, such as the one reported in [47], where the alternation between wetting and drying reproduces the capillary absorption, partial saturation and surface desiccation cycles characteristic of structures exposed to marine aerosols. After each curing period, the samples were removed from their corresponding solution, their initial mass was recorded and dried at 45 ± 2 °C for 12 h until a constant mass was reached. The samples were then placed in a portable and airtight experimental chamber for accelerated exposure to sea breeze (0.8 × 0.6 × 0.4 m) for a total period of 36 h as it can be seen in Figure 5. Exposure was carried out using a sequential protocol with increasing times: a first 12 h misting cycle using natural seawater at a controlled rate of 5 ± 0.5 mL/min, simulating the continuous deposition of marine aerosol; followed by a second cycle of prolonged exposure of 24 h (36 h cumulative). At the end of each stage, the corresponding wet mass was recorded and, subsequently, an intermediate drying was carried out at 45 °C for 12 h to determine the recovered dry mass, allowing the evaluation of absorption and desorption kinetics as a function of time. This scheme, which totaled 36 h of exposure distributed progressively, provided reproducible conditions of accelerated aging and

enabled quantifying the evolution of absorption under controlled wetting-drying cycles. Once the protocol was completed, the samples were subjected to compressive strength, carbonation and chloride penetration tests.

Figure 5. Exposure of samples to accelerated marine breeze conditions.

The portable chamber was equipped with an internal sensor to monitor temperature (35 ± 2 °C) and relative humidity (70% ± 3%), simulating typical coastal conditions of Veracruz, where the average annual ambient temperature is 35 °C and relative humidity ranges between 60% and 80% [48], ensuring conditions conducive to carbonation susceptibility [49].

2.6. Performance evaluation: Substantiation of the response variables

After exposure of the samples to the sea breeze at each curing age, four response variables were selected: compressive strength, water absorption, carbonation depth, and chloride penetration. This selection was based on its relevance for the prediction of the durability of cementitious materials in marine environments, as indicated in [50,51]. Compressive strength was used as a direct indicator of the mechanical integrity of the coating, an essential aspect to ensure its structural stability during service [52]. Water absorption, directly associated with matrix porosity and permeability, was used as a key predictor of durability, since reduced values reflect a denser microstructure with less accessibility to aggressive agents [53]. In addition, the two most relevant chemical degradation mechanisms in the marine environment were evaluated: carbonation, which reduces pH and compromises the protection of reinforcing steel [54,55], and chloride penetration, widely recognized as the main cause of

chloride-induced corrosion in coastal areas [56–58]. Together, these measurements enable us to assess the effectiveness of the coating as a physical-chemical barrier against the main deterioration agents in marine environments. In Figure 6, image A illustrates the procedure for determining carbonation depth and image B for the chloride ions depth.

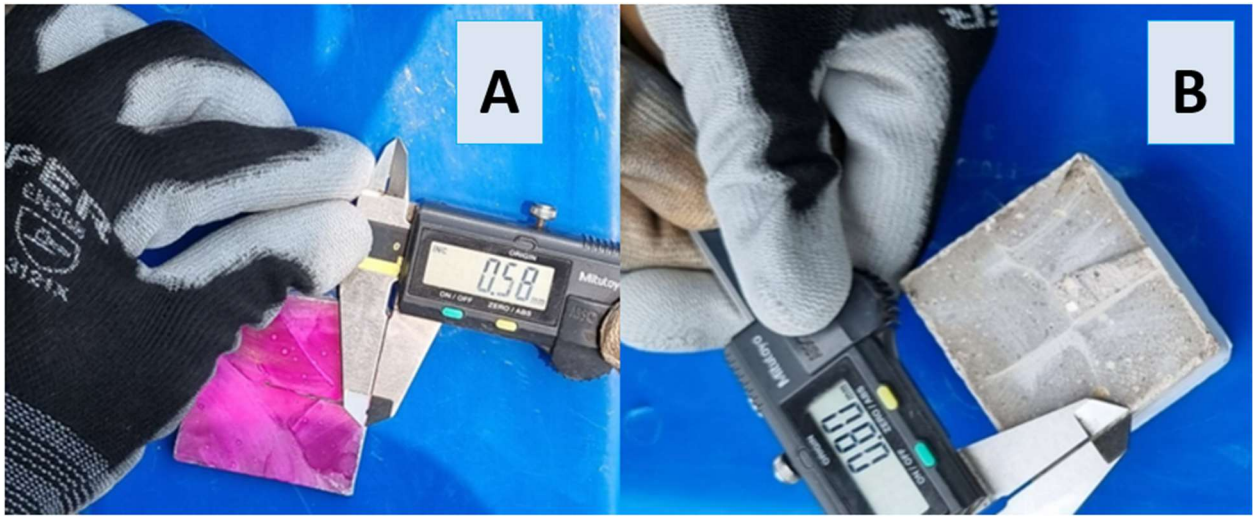

Figure 6. Measurement of the thickness of carbonation and chloride penetration in samples.

The quantification of carbonation depth was performed in accordance with the standardized procedure established in the Mexican Standard NMX-C-515-ONNCCE-2015, which defines the sampling, cutting, and phenolphthalein-based colorimetric criteria for identifying the carbonated front in cementitious materials. The chloride penetration depth was evaluated using a silver nitrate ($AgNO_3$) solution, which enables a clear visual distinction between chloride-free and chloride-contaminated zones through a colorimetric reaction; this procedure was conducted following the experimental methodology reported in [59], which is widely employed for qualitative and comparative assessment of chloride ingress in cement-based materials.

3. Results and discussions

3.1. Density and dry weights of the pastes

Table 5 presents the values of density and average unit dry weight of the different types of samples, considering the three curing ages (28, 56, and 90 days). The variability observed between formulations is directly attributed to differences in the dosage of their components and the inherent density of each material.

Table 5. Density and dry weight of each type of mixtures in the experiment.

Pastes codes	Average dry weight (g)	Density (kg/m^3)
A-1	174	1430
B-1	160	1290
C-1	211	1710
D-1	182	1520
E-1	177	1390
F-1	178	1440
G-1	190	1500

3.2. Critical appearance of pastes after exposure to sea breezes at 90 days

After 36 h of exposure to accelerated sea breezes, the pastes showed significant differences in moisture absorption, shown by visual features in Figure 7.

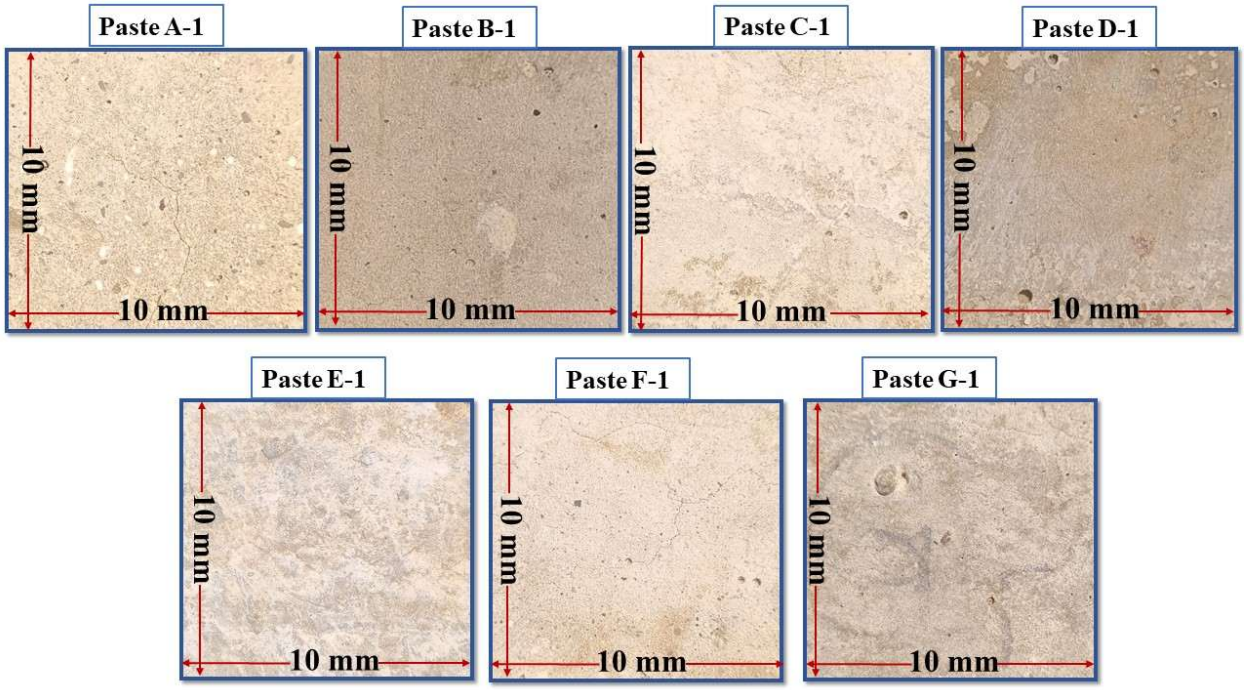

Figure 7. Presentation of sample surfaces after exposure to accelerated sea breezes.

Samples B-1 and D-1 show comparatively high moisture absorption, which is visually reflected in their rougher surface texture and darker coloration (Figure 7). This behavior is consistent with mechanisms reported in the literature, which identify three factors that can contribute to increased water uptake in pumice-based systems: (1) the intrinsically porous nature of pumice, whose vesicular structure (50–200 μm) enhances capillary transport pathways [60,61]; (2) imbalanced SiO_2/CaO ratios, 0.75 in A-1 (SiO_2-deficient) and 1.84 in B-1 (SiO_2-rich), which have been associated with reduced formation of dense C-A-S-H gels and the development of heterogeneous matrices with amorphous domains [62]; and (3) the absence of portlandite [$Ca(OH)_2$] in D-1, a condition that limits

the maintenance of the high alkalinity required for effective pumice dissolution and subsequent reaction product formation [37]. Formulations E-1 and G-1 displayed markedly lower absorption values (35%–40% below the control, according to the results of this study). Literature indicates that such reductions can occur through several mechanisms: The formation of surface-carbonated N-A-S-H gels in low-Ca systems, which produce dense amorphous $CaCO_3$ layers [63]; an optimized pumice/$CaSO_4 \cdot ½H_2O$ ratio (2.5:1), linked to the development of nanostructured ettringite [64]; and pore refinement associated with gypsum ($CaSO_4 \cdot 2H_2O$) precipitation, as previously documented [65].

In the cases of A-1 and F-1 (containing 25% and 20% $Ca(OH)_2$, respectively), the presence of visible microcracks suggests a combined effect consistent with recent findings: excess portlandite can carbonate to form calcite capable of partially blocking pores [66], while SO_4^{2-} ions from hemihydrate can stabilize ettringite at pH levels below 11.5 [67]. These behaviors align with the observations of [14], who reported that $Ca(OH)_2$ contents between 15%–25% enhance matrix densification in supersulfated cements and can improve resistance to chloride ingress and carbonation compared with Portland cement. Regarding the control paste (C-1), its behavior under accelerated marine exposure shows a contrasting trend. At early curing ages, C-1 maintained relatively stable performance and presented limited visual deterioration, indicating an initially strong resistance to saline aerosol. However, after the 90-day curing period and subsequent 36 h exposure to accelerated marine breeze, a noticeable surface color change and the appearance of microcracks were observed. These features suggest that prolonged exposure facilitated the ingress of marine chemical agents, consistent with the known vulnerability of Portland cement matrices to chloride transport and carbonation under sustained aggressive environments. This response reinforces the need for alternative binders with enhanced long-term durability in coastal conditions.

3.3. Compressive strength (CS)

The compressive strengths (CSs) of the samples were measured after the curing periods of 28, 56, and 90 days. For the non-destructive estimation of the compressive strength of the 0.05 × 0.05 × 0.05 m specimens, an analog Schmidt-type sclerometer, previously calibrated with the manufacturer's steel anvil, was used. The equipment had an impact energy of 2.207 J (0.225 kgf·m), operating range of 10–60 MPa, static slider friction 0.5 ± 0.8 N, spring extension 75 mm and spherical tip with a radius of 25 ± 1 mm. Calibration ensured that the rebound readings properly corresponded to the conversion table used (adjusted to kg/cm^2 units). The tests were performed in a vertical descending position (from top to bottom) on the side faces of the cubes. At least nine impacts were made per face, spaced from each other and from the edges.

Although standards such as ASTM C805 recommend ≥0.15 m specimens for rebound hammer testing, the use of this non-destructive method in 0.05 m by side cubes was rigorously validated in this study as follows: a preliminary calibration performed at 28, 56 and 90 days of curing, by correlating rebound readings with destructive compression tests on three specimens of each mixture, showed that the estimated strength of the hammer differed on average only 0.14 MPa from the destructive values. This level of precision was acceptable since our main objective was the comparative evaluation between mixtures and not the determination of absolute values. It should be noted that other studies, such as the one reported by [68], have revealed coefficients of variation up to 20.97% for mixtures with resistances between 14–28 MPa evaluated in a vertical descending position, which favorably contextualizes the reproducibility of our data.

Figure 8 presents the compressive strengths, demonstrating a statistically valid comparative performance in all types of paste and curing ages.

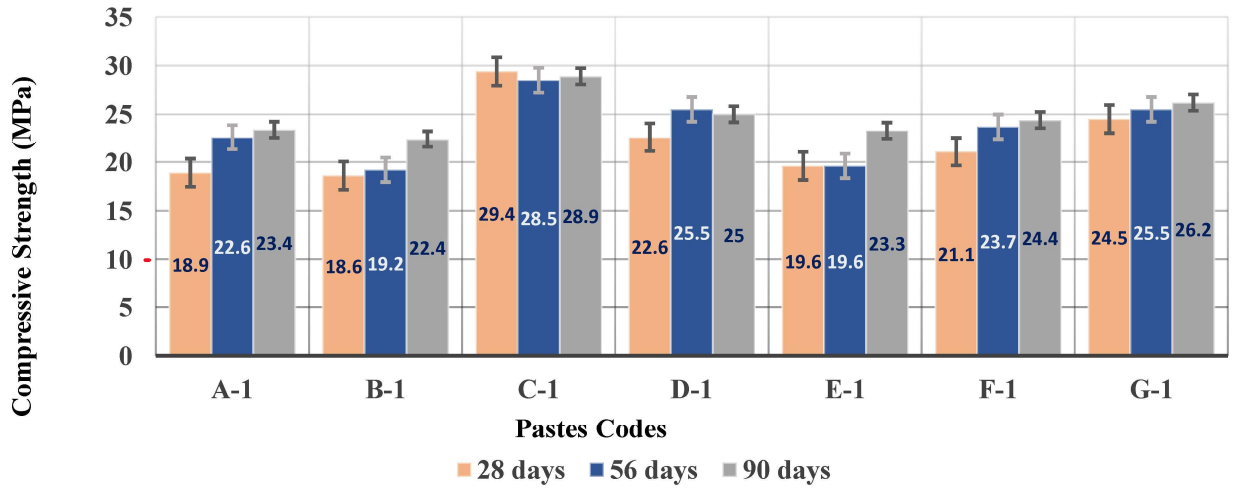

Figure 8. Compressive strength of each type of paste at 28, 56 and 90 days of curing.

According to Figure 8, at 28 days of curing, the supersulfated pastes showed relatively lower mechanical strengths (18.6–24.5 MPa) compared to the Portland cement reference sample C-1 (29.4 MPa). This is consistent with the typical behavior of supersulfated systems, which exhibit slower strength development at early ages due to their distinct hydration kinetics [13]. However, after 56 and 90 days of curing, the supersulfated pastes showed significant strength gains, with formulations such as A-1, E-1, and G-1 increasing by 21%, 19%, and 7%, respectively, between 28 and 90 days, while the reference paste C-1 showed a slight decrease (−1.7%).

The progressive evolution of resistance in supersulfated pastes is consistent with what has been reported in the literature for pozzolana-based systems, where mechanical development at later ages is attributed to the continuous formation of cementitious phases. Studies such as [14,69] have shown that in supersulfated matrices with high silica content, nanostructured etringite and C-A-S-H gels develop that progressively densify the microstructure, reducing porosity and increasing paste cohesion during prolonged hydration.

Additionally, all the formulations developed exceeded the minimum requirement of 15 MPa established by the NMX-C-512-ONNCCE-2022 standard for coating mortars, confirming their technical suitability for the proposed application. To minimize variability, strict controls were implemented that included: (a) maintaining uniform geometry and support conditions, (b) performing measurements exclusively on defect-free surfaces, (c) standardizing the test procedure across all samples and cure ages, and (d) prioritizing comparative analysis over absolute accuracy. This protocol aligns with validated methodologies for the use of rebound hammers in comparative studies with small-format specimens [69].

3.4. Absorption

The absorption percentage allows for a comparison of how much weight the paste gained by absorbing water. The percentage was quantified using the standardized procedure established in the Mexican standard NMX-C-061-ONNCCE-2015, it is indicated by the Eq 1:

$$\text{Absorption (\%)} = \frac{Mh - Ms}{Ms} \times 100\% \quad (1)$$

where: *Mh* = mass of the sample after 72 h of immersion in drinking water at 23 ± 2 °C (g); *Ms* = mass of the sample dried in an oven at 105 ± 5 °C until a constant weight (g) is reached.

This method ensures accurate assessment of the material's absorption capacity, a critical parameter for determining its durability under harsh environmental conditions. Figure 9 shows the variability in the absorption percentage of the samples with respect to curing time.

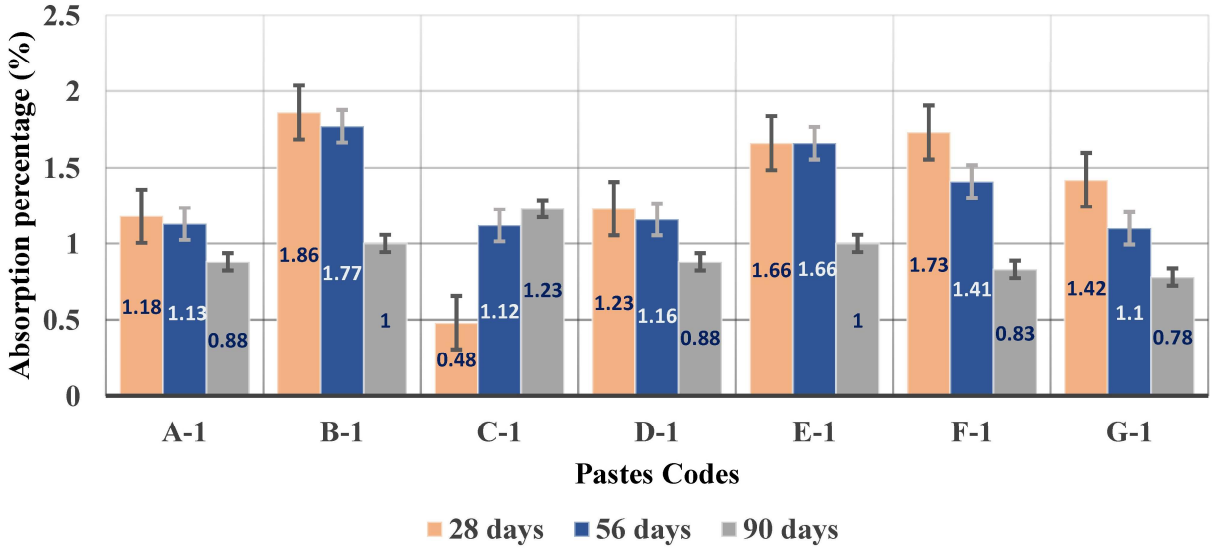

Figure 9. Percentage of moisture absorbed at different curing ages.

At 28 days after curing, the supersulfated samples show an absorption greater than 1.1%, while the C-1 control sample has a lower absorption percentage (0.48%), according to Figure 9. This is because control samples, composed only of Portland cement and water, usually form a homogeneous and compact structure that resists moisture better at an early age. Supersulfated mixtures, on the other hand, according to [70], initially have greater porosity, although this decreases over time thanks to chemical reactions that densify the cement matrix, reducing moisture absorption.

To evaluate the performance of the pastes, the final absorption values (0.5%–1.5% at 90 days) were compared with the durability criteria established in the ACI 201.2R, which recommends that concretes exposed to aggressive environments present absorptions of less than 5%. The results obtained for all supersulfated pastes were well below this threshold, indicating a potential for high durability in marine environments.

3.5. Carbonation

A carbonation test was performed by applying a phenolphthalein solution to the cross-sections of each sample. The solution made it possible to visually identify the carbonated area, which does not change color, and the non-carbonated area, which changes pink. To accurately measure the depth of carbonation, a digital vernier calibrator was used, which measures from the surface of the sample to the boundary of the carbonate zone in millimeters. The measurements were made at various points in the cut sections, determining the maximum depth for each sample. The Figure 10 reports the critical

carbonation depths obtained from multiple measurement points on each specimen, enabling a direct comparison of the progression of carbonation over time.

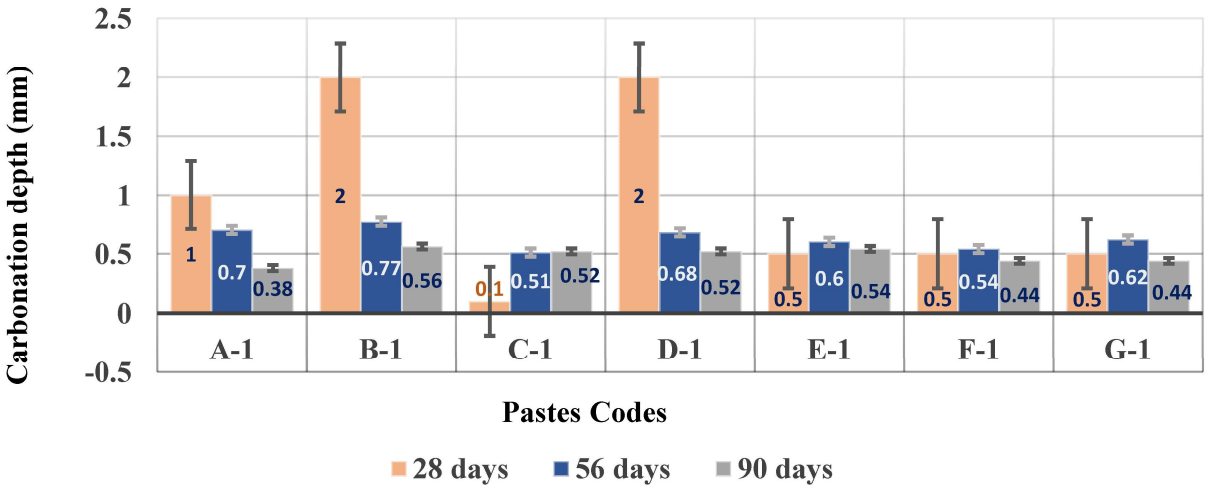

Figure 10. Depth of carbonation of the pastes at different curing ages.

The reference paste C-1 (control paste) initially exhibited a carbonation depth of 0.1 mm. However, this depth tends to increase as the curing age progresses, as shown in Figure 10. Although this paste demonstrates initial resistance to carbonation, such resistance decreases over time due to prolonged exposure to aggressive chemical agents, particularly at advanced curing ages, a phenomenon described by [71]. In contrast, [72] reported that in supersulfated pastes with high silica content, although early carbonation may occur, the system progressively improves due to the formation of highly polymerized C-S-H gels and the development of amorphous phases, such as gelified silica containing finely dispersed calcium carbonate. According to the researchers in [73], this phase, distributed within the matrix because of controlled surface carbonation, contributes to pore sealing through $CaCO_3$ precipitation within the hydrated silica network, forming a physical and chemical barrier against further CO_2 ingress.

The higher dispersion (standard error) observed in the carbonation depth of C-1 paste at 28 days (Figure 10) reflects the initial heterogeneity in CO_2 penetration through the dense and highly alkaline microstructure of Portland cement. This phenomenon, where carbonation begins in a localized manner before establishing a continuous front, has been documented in PC pastes [74]. As exposure progresses, the carbonation front homogenizes, as evidenced by the marked reduction in standard deviation at 56 and 90 days. In contrast, supersulfated pastes showed a more uniform progression from early ages.

It should be noted that the colorimetric method of phenolphthalein, although widely used for carbonation assessments in comparative studies [49,71], is subject to a certain visual subjectivity in the determination of the carbonation front. To mitigate the influence of human factors in this study, a strict protocol was implemented that included: (a) uniform application of the solution by a single operator, (b) depth measurement at least nine points per section using a digital vernier, and (c) reporting of maximum depth as the most conservative parameter for durability evaluation. While alternative methods, such as thermogravimetric analysis (TGA) or electron microscopy offer more accurate quantification of carbonation products, the phenolphthalein method was selected for its practicality, low cost, and ability to provide robust initial and qualitative benchmarking among a large number of

samples, which was the primary focus of this testing phase. Therefore, the reported depth values should be interpreted as reliable indicators of comparative trend between mixtures rather than as absolute measurements of millimeter accuracy. Quantitative characterization of carbonation profiles has been identified as a target for future research.

3.6. Chloride penetration

The chloride penetration depth was measured manually using a digital vernier caliper, from the exposed surface to the boundary marked by the color change. Measurements were taken at multiple points to identify the maximum penetration depth, and these critical values are presented in Figure 11.

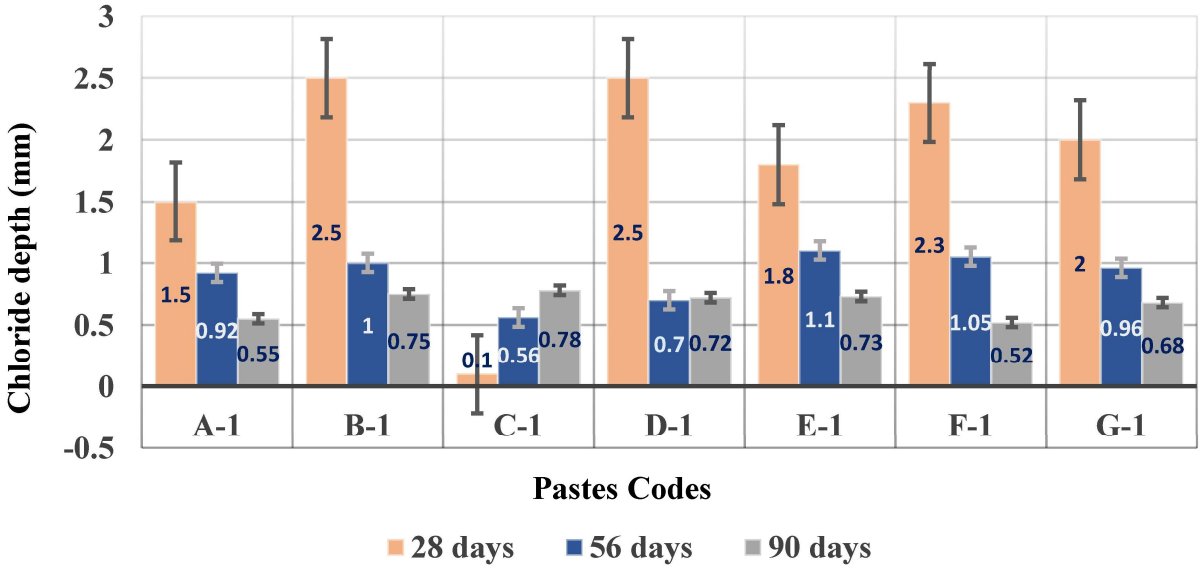

Figure 11. Depth of chloride penetration into the pastes with respect to the curing time.

The chloride penetration results reveal a distinctive temporal trend between the reference paste (C-1) and the supersulfated pastes. The C-1 sample, with its dense C-S-H matrix, showed low initial penetration, consistent with the behavior reported for well-hydrated Portland cement pastes [75]. In contrast, supersulfated pastes exhibited higher initial penetration, a phenomenon documented in the literature and attributed to transient porosity during progressive activation of pozzolan and hemihydrate [46].

However, after 56 days of curing, the supersulfated pastes developed significantly greater resistance to chloride penetration. This continuously improving behavior over time is a fundamental and widely reported characteristic of supersulfated systems. The researchers in [21,76,77] have established that this phenomenon is driven by synergistic mechanisms: (1) pore sealing by growth of nanocrystalline etringite; (2) chemical fixation of chlorides by the formation of Friedel's salt, quantified in high-aluminium system; and (3) continuous microstructural refinement by C-A-S-H geling, which reduces pore size and capillary connectivity.

It should be noted that the $AgNO_3$ method provides a measure of chloride penetration depth rather than continuous concentration profiles. To ensure measurement consistency, a rigorous protocol was implemented: at least nine measurements per sample were taken using a digital caliper by a single operator under controlled lighting conditions, reporting the maximum depth as the most conservative

durability parameter. Consequently, the reported values should be interpreted as robust indicators of comparative trends between mixtures rather than absolute measurements of millimeter precision.

While this approach provides reliable comparative data, estimating a diffusion coefficient under our accelerated exposure regime, which combines wet/dry cycles, would introduce significant uncertainty due to the contribution of non-diffusive transport mechanisms like capillary suction. Therefore, chloride penetration depth was used as a reliable comparative performance indicator, consistent with established practices in accelerated durability studies [78]. For rigorous quantification of diffusion coefficients, methods such as the rapid chloride migration (RCM) test or XRF microanalysis are recommended for future research.

Therefore, the results presented in Figures 8–11 demonstrate that the evolution of the properties of supersulfated pastes progressively improves with curing time, while C-1 control paste shows decreases in its performance in the four response variables after exposure to accelerated sea breezes. In the curing interval of 28 to 90 days, in terms of compressive strength, formulations A-1, B-1, E-1, and F-1 register cumulative increases of more than 15%, reflecting a sustained mechanical development, in contrast to the slight decrease observed in C-1. Regarding the chloride penetration depth, most of the mixtures show significant reductions, particularly A-1, B-1, D-1, F-1, and G-1, with decreases of more than 60%, while C-1 exhibits anomalous increases in all the intervals evaluated. Similarly, formulations A-1, B-1, and D-1 show carbonation reductions greater than 60%, unlike C-1, which again presents atypical increases. In terms of absorption, mixtures B-1, F-1, and G-1 stand out for reductions greater than 45%, while C-1 shows pronounced increases not observed in the rest of the systems. Overall, these results showed a favorable behavior in supersulfated pastes during accelerated exposure in the marine environment, with clear improvements in durability and mechanical performance, while C-1 control paste is distinguished by a progressive deterioration in all the properties evaluated.

3.7. Statistical analysis

It is necessary to highlight that a comprehensive statistical analysis was conducted to evaluate and compare the performance of the different mortar mixtures in terms of four key response variables: CS, carbonation depth, chloride penetration, and water absorption. To ensure the validity and robustness of the statistical inferences, an initial normality assessment was performed on the datasets corresponding to each response variable at the three designated curing ages. This was carried out using the Anderson-Darling normality test, with a significance level (α) set at 5% [79]. The test results confirmed that all datasets followed a normal distribution ($p > 0.05$), thereby fulfilling a fundamental assumption required for parametric inferential methods.

Given the confirmation of normality, a one-way analysis of variance (ANOVA) was subsequently applied to determine whether statistically significant differences existed among the mixture groups for each of the four response variables. The use of ANOVA under conditions of verified normality enhances the reliability of the conclusions drawn, as it minimizes the risk of Type I and Type II errors in hypothesis testing. This statistical approach is particularly appropriate in material performance studies, where the aim is to identify the influence of mixture composition on durability and mechanical properties. Figure 12 illustrates the ANOVA graphs for the evaluated response variables.

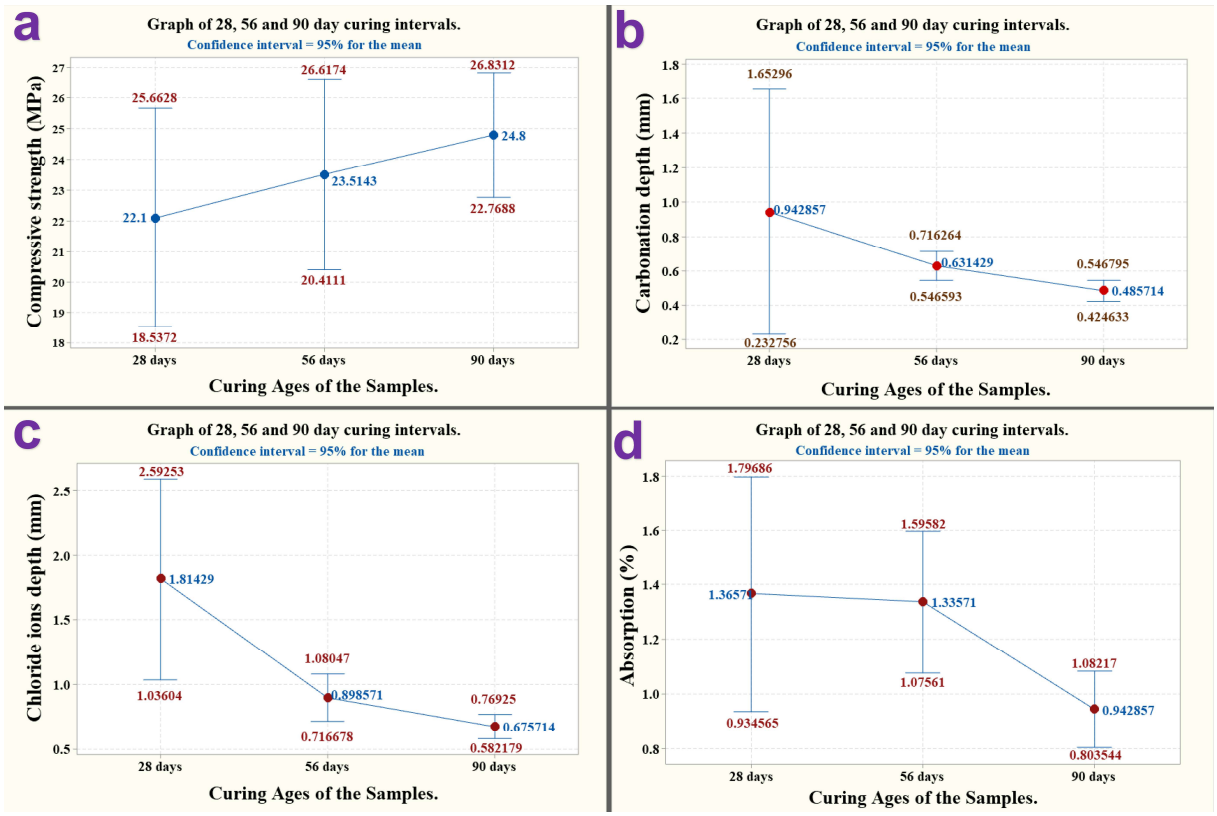

Figure 12. ANOVA of the four response variables in the three ages of curing.

Figure 12 shows that the cure time required for samples to reach adequate strength is statistically 28 days (Figure 12a). At this age, the minimum resistance that any of the pastes can achieve is 18.54 MPa, enough for a non-structural paste used as a coating. Thus, it is concluded that supersulfated pastes achieve adequate mechanical strengths at an early age, making them suitable for non-structural applications such as coatings.

The curing time significantly influences the depth of carbonation. According to Figure 12b, it is observed that the longer the curing time, the greater the resistance of the samples to carbonation. This is reflected in the downward trend of mean carbonation depth values in the confidence interval plot, where carbonation decreases as cure time increases. In addition, it is observed that, after 56 days of curing, there is a smaller deviation in the values of the carbonation depth. Therefore, it is concluded that supersulfated pastes have a good resistance to carbonation after 56 days of curing. According to Figure 12c, a curing time of 28 days is not adequate for pastes to develop good resistance to chloride ion penetration. It can be deduced that the pastes have a greater durability against the penetration of chlorides with a longer curing time, enabling them to develop new chemical mechanisms over time, which help to reduce the speed of corrosion induced by chloride ions. The results observed in Figure 12d stipulate that, with a curing of 90 days, the samples reach a lower percentage of moisture absorption, with an average of 0.943%. Although the standard deviation is greater at 28 days, specimens tend to respond better after 56 days of curing. Table 6 presents the adjusted p-values obtained by the Games-Howell test, which enable us to identify whether there are statistically significant differences between the three cure ages evaluated for each response variable.

Table 6. Games-Howell concurrent tests for mean differences (α = 0.05).

	Level differences	Adjusted P-value
Compressive strength	56–28 days	0.75
	90–28 days	0.288
	90–56 days	0.683
Carbonation depth	56–28 days	0.566
	90–28 days	0.327
	90–56 days	0.015
Chloride ions depth	56–28 days	0.063
	90–28 days	0.027
	90–56 days	0.061
Absorption	56–28 days	0.988
	90–28 days	0.122
	90–56 days	0.024

To assess whether the observed differences between the ages of cure were statistically significant, the Games-Howell post hoc test (α = 0.05) was applied as shown in Table 6, suitable for multiple comparisons between groups with unequal variances. In the case of compressive strength, none of the contrasts between 28, 56, and 90 days presented significant differences ($p > 0.05$), which indicates that the variations detected experimentally correspond to fluctuations of the system and not to statistically distinguishable changes between ages. For carbonation depth, only the 90–56-day contrast showed statistical significance ($p = 0.015$), evidencing an additional reduction in carbonation between these ages that was not present in the previous intervals. In chloride penetration, the contrast 90–28 days was significant ($p = 0.027$), indicating a marked decrease in the depth of chloride entry between these ages; however, the 56–28 and 90–56-day intervals did not reach significance, suggesting that the greatest change occurs in the transition between 28 and 90 days. Finally, in absorption, only the contrast 90–56 days was significant ($p = 0.024$), confirming a statistically consistent reduction in absorption between these ages, while the differences between 28 and 56 days were not significant. Overall, these results showed that the effects of prolonged curing are not uniformly manifested in all the properties evaluated: While compression did not show statistically detectable changes, properties associated with durability (carbonation, chlorides and absorption) showed significant improvements in advanced stages of curing.

Therefore, according to the statistical analysis, the age of 56 days represents the minimum time from which the microstructures of the supersulfated pastes begin to consolidate and resist the chemical attack of the sea breeze in the coastal region of Veracruz. In addition, the following is observed: Supersulfated pastes develop adequate mechanical resistance and durability to resist the chemical attack of the sea breeze from the age of 56 days of curing. Compared to the control mixture, the supersulfated pastes that demonstrated the best performance against chemical attacks and durability, with relatively low standard deviations, were E-1 (30% Portland cement, 50% activated pumice, 20% $CaSO_4 \cdot ½H_2O$) and G-1 pastes (40% Portland cement, 40% activated pumice (with NaOH), 20% $CaSO_4 \cdot ½H_2O$).

4. Conclusions

This study demonstrates that supersulfated pastes formulated with locally sourced pumice and activated through a two-stage alkaline process constitute a high-performance and sustainable alternative to Portland cement for marine-exposed coatings. The most significant results, which directly respond to the objective of evaluating its durability and mechanical behavior, are summarized below:

- Unlike Portland cement control paste, which did not show a significant gain in strength and a slight decrease at 90 days of curing (−1.7%), supersulfated formulations showed continuous mechanical development, achieving strength increases of up to 21% between 28 and 90 days.
- In terms of absorption percentage, supersulfated pastes performed better than control paste, especially after 56 days of curing. Although initially showing greater absorption due to their early porosity, these pastes managed to achieve final values of 0.5%–1.5% at 90 days, well below the 5% limit recommended by ACI 201.2R for materials exposed to aggressive environments. In contrast, Portland control pasta did not experience significant improvements with advanced age.
- As for carbonation, the control paste showed the lowest initial depth, but progressively increased its vulnerability over time. Supersulfated pastes, on the other hand, showed a sustained reduction in carbonation after 56 days. This behavior confirms that pumicite-based supersulfated systems develop more stable and effective physical-chemical barriers against CO_2 and humidity in marine environments.
- The supersulfated pastes developed a markedly higher resistance to chloride penetration. Formulations such as A-1, B-1 and G-1 reduced chloride input by more than 60% during the curing period, while control paste experienced anomalous increases under the same exposure conditions.
- The statistical analysis showed that, from 56 days, the activated pumice systems reached a consolidated microstructure that significantly reduced the depth of carbonation (reductions greater than 60% in A-1 and B-1) and water absorption (reductions greater than 45% in B-1 and G-1).
- By integrating the four durability indicators, such as compressive strength, water absorption, carbonation depth, and chloride penetration, the E-1 and G-1 formulations demonstrated the most robust overall performance.

In summary, the results validate that pumice-based supersulfated pastes not only meet the technical requirements for coastal protective coatings, but can exceed the long-term durability and mechanical performance of Portland cement. These results position activated pumice as a viable local resource to develop high-resilience and low-carbon cementitious systems, adapted to aggressive marine environments.

5. Future research

Based on our findings, several research directions are proposed to address limitations and further advance the understanding of supersulfated pumice-based pastes:

1. A comprehensive analysis using Scanning Electron Microscopy (SEM), coupled with Energy-Dispersive X-ray Spectroscopy (EDS), and XRD is essential to visually confirm and quantify the formation of nanostructured ettringite, C-A-S-H gels, and Friedel's salt in NaOH-activated pumice supersulfated pastes. Such characterization would provide direct evidence of the microstructural mechanisms inferred from the macroscopic durability results.

2. To complement the comparative penetration-depth measurements used in this study, researchers should incorporate Rapid Chloride Migration (RCM) testing and water sorptivity measurements to

determine the apparent diffusion coefficient and capillary absorption rate, respectively. These parameters would enable more rigorous and quantitative service-life modeling.

3. Validating the accelerated laboratory results through prolonged exposure in a real marine environment along the coast of Veracruz is essential. This would enable the evaluation of performance under natural environmental cycles, including UV radiation, tidal splash, and thermal fluctuations.

4. Further investigation is required to determine the optimum NaOH concentration and the most effective pumice/hemihydrate ratio to maximize reaction efficiency, microstructural refinement, and long-term durability.

5. Conducting a cradle-to-gate LCA would quantify the environmental benefits of the developed pumice-based supersulfated system, particularly in terms of CO_2 emission reduction and energy savings, compared with conventional Portland cement coatings.

Use of AI tools declaration

The authors declare they have not used Artificial Intelligence (AI) tools in the creation of this article.

Acknowledgments

This research was supported by a scholarship granted by the Government of Mexico through the Secretaría de Ciencia, Humanidades, Tecnología e Innovación (Secihti). The experimental work was conducted at the Civil Engineering Laboratory of National Technological Institute of Mexico, Misantla Campus, Veracruz.

Sincere gratitude to Dr. David Reyes Gonzalez for his significant guidance and continued support throughout the development of this project. Special thanks are extended to Dr. Rodrigo Vivar Ocampo (Renewable Energy Department, Autonomous University of Baja California) for his valuable feedback, and to Dr. Gustavo Martínez Castellanos and Dr. Pablo Julian Lopez-Gonzalez for their helpful comments during the manuscript revision.

Author contributions

Conceptualization, methodology, experimentation, and writing of the original draft: Kenson Noel; supervision, review, and editing: David Reyes-Gonzalez; additional review and feedback: Gustavo Martinez Castellanos, Rodrygo Vivar-Ocampo, and Pablo Julian Lopez-Gonzalez. All authors have read and agreed to the published version of the manuscript.

Conflict of interest

The authors declare no conflict of interest.

References

1. Kim IS, Choi SY, Yang EI (2018) Evaluation of durability of concrete substituted heavyweight waste glass as fine aggregate. *Constr Build Mater* 184: 269–277. https://doi.org/10.1016/j.conbuildmat.2018.06.221

2. Paul SC, van Zijl GPAG, Šavija B (2020) Effect of fibers on durability of concrete: A practical review. *Materials* 13: 4562. https://doi.org/10.3390/ma13204562
3. Wong LS (2022) Durability performance of geopolymer concrete: A review. *Polymers* 14: 868. https://doi.org/10.3390/polym14050868
4. Maddalena R, Roberts JJ, Hamilton A (2018) Can Portland cement be replaced by low-carbon alternative materials? A study on the thermal properties and carbon emissions of innovative cements. *J Clean Prod* 186: 933–942. https://doi.org/10.1016/j.jclepro.2018.02.138
5. Askarian M, Fakhretaha Aval S, Joshaghani A (2018) A comprehensive experimental study on the performance of pumice powder in self-compacting concrete (SCC). *J Sustain Cem Based Mater* 7: 340–356. https://doi.org/10.1080/21650373.2018.1511486
6. Abbas R, Abdelzaher MA, Shehata N, et al. (2024) Production, characterization and performance of green geopolymer modified with industrial by-products. *Sci Rep* 14: 5104. https://doi.org/10.1038/s41598-024-55494-8
7. Singh NB, Middendorf B (2020) Geopolymers as an alternative to Portland cement: an overview. *Constr Build Mater* 237: 117455. https://doi.org/10.1016/j.conbuildmat.2019.117455
8. Erdem TK, Meral Ç, Tokyay M, et al. (2007) Use of perlite as a pozzolanic addition in producing blended cements. *Cem Concr Compos* 29: 13–21. https://doi.org/10.1016/j.cemconcomp.2006.07.018
9. Chihaoui R, Siad H, Senhadji Y, et al. (2022) Efficiency of natural pozzolan and natural perlite in controlling the alkali-silica reaction of cementitious materials. *Case Stud Constr Mater* 17: e01246. https://doi.org/10.1016/j.cscm.2022.e01246
10. Stefanidou M (2023) Substituting natural pozzolan with artificial derived from industrial perlite waste for mortar production. In: Jędrzejewska A, Kanavaris F, Azenha M, et al. *International RILEM Conference on Synergising Expertise towards Sustainability and Robustness of Cement-based Materials and Concrete Structures*, Cham: Springer. https://doi.org/10.1007/978-3-031-33211-1_1
11. Ban J, Wu Q, Yu Z, et al. (2024) Mechanisms on the inhibition of alkali-silica reaction in supersulfated cement. *Cem Concr Compos* 145: 105320. https://doi.org/10.1016/j.cemconcomp.2023.105320
12. Zokaei S, Siad H, Lachemi M, et al. (2025) Enhancing the self-healing properties of engineered cementitious composites by the application of super-sulfated cement. *Mag Concr Res* 77: 42–55. https://doi.org/10.1680/jmacr.23.00361
13. Wu Q, Xue Q, Yu Z (2021) Research status of super sulfate cement. *J Clean Prod* 294: 126228. https://doi.org/10.1016/j.jclepro.2021.126228
14. Cabrera-Luna K, Maldonado-Bandala EE, Nieves-Mendoza D, et al. (2021) Supersulfated cements based on pumice with quicklime, anhydrite and hemihydrate: Characterization and environmental impact. *Cem Concr Compos* 124: 104236. https://doi.org/10.1016/j.cemconcomp.2021.104236
15. Ma W, Zheng J, Feng S, et al. (2025) Evaluation on the long-term properties of the steel fiber-reinforced supersulfated cement mortar in seawater environment and performance enhancement through alkalinity regulation. *J Build Eng* 112: 113596. https://doi.org/10.1016/j.jobe.2025.113596

16. Szabó R, Kristály F, Nagy S, et al. (2023) Reaction, structure and properties of eco-friendly geopolymer cement derived from mechanically activated pumice. *Ceram Int* 49: 6756–6763. https://doi.org/10.1016/j.ceramint.2022.10.204
17. Zhao Y, Zhao W, Wei W, et al. (2024) Effect of styrene-acrylic latex on physical-mechanical properties and microstructure of sulphoaluminate cement paste. *ZKG Int* 77: 50–59.
18. Mei J, Deng C, Hu X, et al. (2023) Resistance of polymer modified calcium sulfoaluminate cement to sulphate attack. *ZKG Int* 76: 54–61.
19. Mei J, Yuan C, Niu Y, et al. (2024) Sulfate resistance of alkali-activated slag/metakaolin/fly ash cementitious materials. *ZKG Int* 77: 50–59.
20. Moolchandani K (2025) Advancements in pumice-based concrete: A comprehensive review. *Next Mater* 8: 100646. https://doi.org/10.1016/j.nxmate.2025.100646
21. Poupelloz E, Gauffinet S, Nonat A (2020) Study of nucleation and growth processes of ettringite in diluted conditions. *Cem Concr Res* 127: 105915. https://doi.org/10.1016/j.cemconres.2019.105915
22. Zeyad AM, Shubaili M, Abutaleb A (2023) Using volcanic pumice dust to produce high-strength self-curing concrete in hot weather regions. *Case Stud Constr Mater* 18: e01927. https://doi.org/10.1016/j.cscm.2023.e01927
23. Sun H, Lin T, Zhuo K Q, et al. (2024) Sulfate optimization in ettringite rich cements by SO_3/Al_2O_3 molar ratio: A comparative study of calcium sulfoaluminate and aluminate cements. *Case Stud Constr Mater* 21: e03701. https://doi.org/10.1016/j.cscm.2024.e03701
24. Bergna D, Varila T, Romar H, et al. (2018) Comparison of the properties of activated carbons produced in one-stage and two-stage processes. *C* 4: 41. https://doi.org/10.3390/c4030041
25. Nyangi P (2025) Chemical characterization of pumice material sourced from Mbeya, Tanzania. *MUST*. Available from: https://repository.must.ac.tz/handle/123456789/304.
26. Sahakyan E, Arzumanyan A, Muradyan N (2022) Inorganic polymeric materials based on natural silicate and aluminosilicate raw materials. *Key Eng Mater* 906: 1–6. https://doi.org/10.4028/www.scientific.net/KEM.906.1
27. Rakhimova NR, Morozov VP, Eskin AA (2021) Phase formation behavior of alkali-activated calcined clays: Effects of the reactive phase and NaOH concentration. *Geosyst Eng* 24: 238–246. https://doi.org/10.1080/12269328.2021.1961615
28. Tsintskaladze G, Kordzakhia T, Skhvitaridze R, et al. (2024) Physical and chemical characteristics of pumice from some regions of Georgia and the prospects for its use in lightweight concrete with environmental advantages, In: Jeswani H, *Environmental Technology and Sustainability*, Boca Raton: Apple Academic Press, 247–256. https://doi.org/10.1201/9781003397960-16
29. Cabrera-Luna K, Perez-Cortes P, Escalante Garcia JI (2022) Pumice-based supersulfated cements in mortars: Effects of pumice fineness and activator ratio on physical and environmental characteristics. *Constr Build Mater* 342: 127947. https://doi.org/10.1016/j.conbuildmat.2022.127947
30. Jwaida Z, Dulaimi A, Mashaan N, et al. (2023) Geopolymers: The green alternative to traditional materials for engineering applications. *Infrastructures* 8: 98. https://doi.org/10.3390/infrastructures8060098
31. Komaei A, Saeedi A (2025) Pumicite-based geopolymer optimization for sustainable soil stabilization. *J Mater Civ Eng* 37. https://doi.org/10.1061/JMCEE7.MTENG-19308

32. Bo Q (2018) Temperature effect on performance of Portland cement versus advanced hybrid cements and alkali-fly ash cement. PhD Thesis, Universidad Politécnica de Madrid. https://doi.org/10.20868/UPM.thesis.49698
33. Zhou Y, Peng Z, Chen L, et al. (2021) The influence of two types of alkali activators on the microstructure and performance of supersulfated cement concrete: mitigating the strength and carbonation resistance. *Cem Concr Compos* 118: 103947. https://doi.org/10.1016/j.cemconcomp.2021.103947
34. Provis JL, Van Deventer JSJ (2014) *Alkali Activated Materials: State-of-the-Art Report, RILEM TC 224-AAM*, Dordrecht: Springer. https://doi.org/10.1007/978-94-007-7672-2
35. Mansor AM, Borg RP, Hamed AMM, et al. (2018) The effects of water-cement ratio and chemical admixtures on the workability of concrete. *IOP Conf Ser Mater Sci Eng* 442: 012017. https://doi.org/10.1088/1757-899X/442/1/012017
36. Doan T, Arulrajah A, Horpibulsuk S, et al. (2024) Low-carbon metakaolin precursor for one-part and two-part geopolymer activation of demolition wastes. *Constr Build Mater* 442: 137663. https://doi.org/10.1016/j.conbuildmat.2024.137663
37. Provis JL, Bernal SA (2014) Geopolymers and related alkali-activated materials. *Annu Rev Mater Res* 44: 299–327. https://doi.org/10.1146/annurev-matsci-070813-113515
38. Li X, Yu X, Zhao Y, et al. (2022) Effect of initial curing period on the behavior of mortar under sulfate attack. *Constr Build Mater* 326: 126852. https://doi.org/10.1016/j.conbuildmat.2022.126852
39. Ghazy MF, Abd Elaty MA, Mostafa SM (2022) Properties of one-part versus two-part geopolymers composites—A review. *Am J Eng Res* 11: 1–14.
40. Mahendra K, Narasimhan MC (2023) One part alkali-activated materials for construction—A review. *Mater Today Proc* 93: 182–188. https://doi.org/10.1016/j.matpr.2023.07.116
41. NASA (2025) Sea surface salinity from space. Available from: https://salinity.oceansciences.org/science-salinity.htm (accessed Jul. 28, 2025).
42. Roger Williams University (2025) Salinity patterns, Introduction to Oceanography Cap(5.3.). Available from: https://rwu.pressbooks.pub/webboceanography/chapter/5-3-salinity-patterns/ (accessed Jul. 28, 2025).
43. NRMCA (2020) Concrete in Practice: CIP 13—Chloride Limits in Concrete. Available from: https://www.nrmca.org/wp-content/uploads/2020/04/Tip13w.pdf (accessed Jul. 28, 2025).
44. California Department of Transportation (Caltrans) (2020) Corrosion Threshold Guidelines. Available from: https://dot.ca.gov/-/media/dot-media/programs/engineering/documents/mets/corrosion-guidelines-a11y.pdf (accessed Jul. 28, 2025).
45. Weather Spark (2025) El clima y el tiempo promedio en todo el año en Veracruz México. Available from: https://es.weatherspark.com/y/8657/Clima-promedio-en-Veracruz-M%C3%A9xico-durante-todo-el-a%C3%B1o (accessed Jul. 28, 2025).
46. Pinto SR, Angulski da Luz C, Munhoz GS, et al. (2020) Resistance of phosphogypsum-based supersulfated cement to carbonation and chloride ingress. *Constr Build Mater* 263: 120640. https://doi.org/10.1016/j.conbuildmat.2020.120640
47. He Y, Li Y, Jia J, et al. (2024) Effect of seawater dry-wet cycling on the durability of concrete repair materials. *J Sustain Cem Based Mater* 13: 402–415. https://doi.org/10.1080/21650373.2023.2279288

48. Weatherspark (2024) El clima y el tiempo promedio en todo el año en Nautla. Available from: https://es.weatherspark.com/y/8752/Clima-promedio-en-Nautla-M%C3%A9xico-durante-todo-el-a%C3%B1o (accessed Jul. 07, 2024).
49. Chen Y, Liu P, Yu Z (2018) Effects of environmental factors on concrete carbonation depth and compressive strength. *Materials* 11: 2167. https://doi.org/10.3390/ma11112167
50. Pratiwi WD, Putra FDD, Triwulan, et al. (2021) A review of concrete durability in marine environment. *IOP Conf Ser Mater Sci Eng* 1175: 012018. https://doi.org/10.1088/1757-899X/1175/1/012018
51. Alexander M, Beushausen H (2019) Durability, service life prediction, and modelling for reinforced concrete structures—Review and critique. *Cem Concr Res* 122: 17–29. https://doi.org/10.1016/j.cemconres.2019.04.018
52. Lee T, Kim D, Cho S, et al. (2025) Advancements in surface coatings and inspection technologies for extending the service life of concrete structures in marine environments: A critical review. *Buildings* 15: 304. https://doi.org/10.3390/buildings15030304
53. Ortiz-Marqués A, Caldevilla P, Goldmann E, et al. (2025) Porosity and permeability in construction materials as key parameters for their durability and performance: A review. *Buildings* 15: 3422. https://doi.org/10.3390/buildings15183422
54. Al Fuhaid AF, Niaz A (2022) Carbonation and corrosion problems in reinforced concrete structures. *Buildings* 12: 586. https://doi.org/10.3390/buildings12050586
55. Melchers RE, Richardson PJ (2023) Carbonation, neutralization, and reinforcement corrosion for concrete in long-term atmospheric exposures. *Corrosion* 79: 395–404. https://doi.org/10.5006/4224
56. Zhao R, Li C, Guan X (2024) Advances in modeling surface chloride concentrations in concrete serving in the marine environment: A mini review. *Buildings* 14: 1879. https://doi.org/10.3390/buildings14061879
57. Ali M, Li S, Shahzad M, et al. (2024) A review on chloride induced corrosion in reinforced concrete structures: Lab and in situ investigation. *RSC Adv* 14: 37252–37271. https://doi.org/10.1039/D4RA05506C
58. Wu L, Xia Y, Shi F (2025) Experimental and numerical simulation research on chloride ion corrosion of concrete in a marine silt environment. *Int J Civ Eng* 23: 2021–2035. https://doi.org/10.1007/s40999-025-01133-w
59. Vieira Pontes C, Costa Reus G, Calvo A, et al. (2021) Procedimento para detectar a penetração de cloretos com nitrato de prata em concreto carbonatado. *Rev ALCONPAT* 11: 164–177. https://doi.org/10.21041/ra.v11i2.480
60. Chambua ST, Jande YAC, Machunda RL (2021) Strength and durability properties of concrete containing pumice and scoria as supplementary cementitious material. *Adv Mater Sci Eng* 2021: 5578870. https://doi.org/10.1155/2021/5578870
61. Karthika RB, Vidyapriya V, Nandhini Sri KV, et al. (2021) Experimental study on lightweight concrete using pumice aggregate. *Mater Today Proc* 43: 1606–1613. https://doi.org/10.1016/j.matpr.2020.09.762
62. Bagci C, Kafkas D, Samuel DM, et al. (2024) Sustainable activation of pumice with partially variable substitutions of metakaolin and/or fumed silica. *Int J Appl Ceram Technol* 21: 818–828. https://doi.org/10.1111/ijac.14545

63. Zeyad AM, Khan AH, Tayeh BA (2020) Durability and strength characteristics of high-strength concrete incorporated with volcanic pumice powder and polypropylene fibers. *J Mater Res Technol* 9: 806–818. https://doi.org/10.1016/j.jmrt.2019.11.021
64. Sonebi M, Abdalqader A, Fayyad T, et al. (2020) Optimisation of rheological parameters, induced bleeding, permeability and mechanical properties of supersulfated cement grouts. *Constr Build Mater* 262: 120078. https://doi.org/10.1016/j.conbuildmat.2020.120078
65. Maldonado Bandala EE, Cabrera Luna K, Escalante Garcia JI, et al. (2018) Resistance to compression and microstructure of concrete manufactured with supersulfated cements-based materials of volcanic origin exposed to a sulphate environment. *Rev ALCONPAT* 9: 106–116. https://doi.org/10.21041/ra.v9i1.374
66. Hegazy A, Khalil A, El-Alfi E, et al. (2019) Durability of supersulphated cement pastes activated with Portland cement in magnesium chloride solution. *Egypt J Chem*. https://doi.org/10.21608/ejchem.2019.6563.1579
67. Trentin PO, Perardt M, Medeiros-Junior RA (2022) Ettringite instability analysis in the hydration process of the supersulfated cement. *J Therm Anal Calorim* 147: 6631–6642. https://doi.org/10.1007/s10973-021-11005-9
68. Atoyebi OD, Ayanrinde OP, Oluwafemi J (2019) Reliability comparison of Schmidt rebound hammer as a non-destructive test with compressive strength tests for different concrete mix. *J Phys Conf Ser* 1378: 032096. https://doi.org/10.1088/1742-6596/1378/3/032096
69. Mengistu GM, Gyurkó Z, Nemes R (2023) The influence of the rebound hammer test location on the estimation of compressive strength of a historical solid clay brick. *Solids* 4: 71–86. https://doi.org/10.3390/solids4010005
70. Kabay N, Miyan N, Özkan H (2021) Utilization of pumice powder and glass microspheres in cement mortar using paste replacement methodology. *Constr Build Mater* 282: 122691. https://doi.org/10.1016/j.conbuildmat.2021.122691
71. Li D, Li L, Wang X (2019) Chloride diffusion model for concrete in marine environment with considering binding effect. *Mar Struct* 66: 44–51. https://doi.org/10.1016/j.marstruc.2019.03.004
72. Chen H, Zhou Y, Zhang Y, et al. (2025) Improving the carbonation resistance of supersulfated cement by nano SiO_2 and silica fume. *Cem Concr Compos* 158: 105984. https://doi.org/10.1016/j.cemconcomp.2025.105984
73. Sohail MG, Kahraman R, Al Nuaimi N, et al. (2021) Durability characteristics of high and ultra-high performance concretes. *J Build Eng* 33: 101669. https://doi.org/10.1016/j.jobe.2020.101669
74. Wang X, Yang Q, Peng X, et al. (2024) A review of concrete carbonation depth evaluation models. *Coatings* 14: 386. https://doi.org/10.3390/coatings14040386
75. Bameri M, Rashidi S, Mohammadhasani M, et al. (2022) Evaluation of mechanical and durability properties of eco-friendly concrete containing silica fume, waste glass powder, and ground granulated blast furnace slag. *Adv Mater Sci Eng* 2022: 2730391. https://doi.org/10.1155/2022/2730391
76. Long WJ, Feng TT, Xing F, et al. (2022) Investigation on chloride binding capacity and stability of Friedel's salt in graphene oxide reinforced cement paste. *Cem Concr Compos* 132: 104603. https://doi.org/10.1016/j.cemconcomp.2022.104603
77. Han Y, Xia J, Chang H, et al. (2021) The influence mechanism of ettringite crystals and microstructure characteristics on the strength of calcium-based stabilized soil. *Materials* 14: 1359. https://doi.org/10.3390/ma14061359.

78. Sai KPP, Rao BK, Veerendra GTN, et al. (2024) A critical examination on service life prediction of RC structures with respect to chloride-ion penetration. *J Bio Tribocorros* 10: 5. https://doi.org/10.1007/s40735-023-00808-y
79. Law AM (2015) *Simulation Modeling and Analysis*, 5 Eds., New York: McGraw-Hill Education.

AIMS Press